SAND99-0953C

P2-128

SIMULTANEOUS NUCLEAR REACTION ANALYSIS OF BORON AND PHOSPHORUS IN THIN BOROPHOSPOSILICATE GLASS FILMS USING (α,p) REACTIONS

D. S. Walsh and B. L. Doyle
Sandia National Laboratories, P.O Box 5800, Albuquerque, NM 87185-1056 U.S.A

This work performed by Sandia National Laboratories. Sandia is a multi-program laboratory operated by Sandia Corporation, a Lockheed Martin Company, for the United States Department of Energy under contract DE-AC04-94AL85000.

Abstract:
A method combining (α,p) NRA and ellipsometry has been developed for measuring the Boron and Phosphorus content of borophosphosilicate glass (BPSG) used for interlevel dielectrics in integrated circuits. Yields from the $^{31}P(\alpha,p_0)^{34}S$ (Q = 0.63 MeV) and $^{10}B(\alpha,p_0)$ ^{13}C (Q = 4.06 MeV) reactions are coupled with ellipsometry thickness measurements to calculate the average atomic percent of B and P in the film. Due to the relatively low Q value of the $^{31}P(\alpha,p_0)^{34}S$ reaction and the thickness range of the glass films (≤1.2 micrometers) we analyze, fairly high energy alpha particles, and Mylar range foils on the detector are required. Alpha energy, detector angle and range foil thickness were determined by reaction yields and the need to separate the yield peaks of interest from competing (α,p) reactions and backscattered alphas. We have determined that 6.0 MeV incident alphas with a detector angle of 135° and about 100 micrometers of Mylar range foil are optimum for our system. The yield for the $^{10}B(\alpha,p_0)$ ^{13}C reaction is quite constant in our energy range of interest (~5.8 to 6 MeV) but the yield for the $^{31}P(\alpha,p_0)^{34}S$ is not. Consequently, a simple conversion from "standard" BPSG reference samples (independently quantified by ICP mass spectrometry) is adequate to calculate a film's %B content. The %P calculation is more complex, involving a three–dimensional fit of the P yield data and measured film thickness to the film %P content. This fit is based upon yield data from a matrix of "standard" film samples. The technique is sensitive to 0.1% with an accuracy of ±3 to ±10% depending on the sample. This measurement method is used routinely at Sandia National Laboratories in support of our fabrication process lines.

PACS: 25.55.-e, 25.55.C
Keywords: nuclear reaction analysis, (α,p), borophosphosilicate glass

Corresponding Author:
David S. Walsh
MS 1056
Sandia National Laboratories
Albuquerque, NM U.S.A 87185-1056
Telephone: (505)844-9590
Fax: (505)844-7775
e-mail: dswalsh@sandia.gov

Introduction:

Borophosphosilicate glass (BPSG) is an important component of silicon based semiconductor technology. The main function of BPSG traditionally is as an interlevel dielectric capable of filling gaps and planarizing local interlevel surfaces, but it is also occasionally used as a passivation cap layer in CMOS devices [1,2]. The addition of B and P dopants in the form of B_2O_3 and P_2O_5 while depositing silicon dioxide films allow the films to make the transition to smooth flowing glass during a high temperature anneal (traditionally >900°C) processing step. Studies have shown that a critical minimum phosphorous concentration is necessary to activate the boron oxide in the deposition process and effect viscosity and the glass transition temperature. Also, there exists an optimum phosphorus concentration for any given boron concentration to achieve the lowest possible viscosity, the minimum flow angles, and hence the best gap-filling glass. Above this optimum phosphorus concentration the viscosity and flow angles increase [2,3].

The smaller device geometry and use of Ti-silicide in modern silicon devices have resulted in more stringent thermal processing budgets for such devices. This means that minimum viscosity and flow angle must now be obtained in the 700° to 850° C range[3], which in turn requires better understanding of the chemistry of BPSG deposition and more precise control of boron and phosphorus concentrations in the films. Periodic monitoring of the deposition process via post-deposition, off-line analysis of the boron and phosphorus concentrations in BPSG is common in the semiconductor industry. Several techniques have been used for this purpose: Inductively Coupled Plasma mass Spectrometry (ICPS), Secondary Ion Mass Spectrometry (SIMS), electron microprobe x-ray analysis and infrared spectrometry.

DISCLAIMER

This report was prepared as an account of work sponsored by an agency of the United States Government. Neither the United States Government nor any agency thereof, nor any of their employees, make any warranty, express or implied, or assumes any legal liability or responsibility for the accuracy, completeness, or usefulness of any information, apparatus, product, or process disclosed, or represents that its use would not infringe privately owned rights. Reference herein to any specific commercial product, process, or service by trade name, trademark, manufacturer, or otherwise does not necessarily constitute or imply its endorsement, recommendation, or favoring by the United States Government or any agency thereof. The views and opinions of authors expressed herein do not necessarily state or reflect those of the United States Government or any agency thereof.

DISCLAIMER

Portions of this document may be illegible in electronic image products. Images are produced from the best available original document.

The Ion Beam Materials Research Lab (IBMRL) at Sandia National Laboratories was asked to develop an ion beam based technique for measuring boron and phosphorus concentrations in the thin BPSG dielectric films produced by our fab during CMOS processing. Phosphorus [4-6] and boron [7-9] have often been detected and profiled using a variety of resonant (p,γ), (p,α) and even (α,p) nuclear reactions. The (α,p) reactions are generally considered less useful for the analysis of light elements than proton or deuteron induced reactions for several reasons. First, most of the light element (α,p) reactions have negative or very low Q-values. Second, the cross-sections are generally small, especially below 2 MeV where many small accelerators operate. Third, the cross-sections are generally full of numerous narrow resonances which are neither narrow enough, nor separated far enough from neighboring resonances to be of much use for depth profiling.

Exceptions to the rule do exist however, and McIntyre and co-workers have demonstrated the ability to profile both phosphorus and boron using (α,p) reaction resonances [5,9]. Like all resonant techniques these require the use of multiple incident ion energies to profile the element in question. For our particular application we were looking for a quick, simple, technique (i.e., using a single incident ion energy to detect both boron and phosphorus) due to cost, time and manpower constraints. We have in the past used enhanced Rutherford Backscattering Spectrometry (RBS) to measure the boron and carbon concentrations in thin boron-carbon films deposited upon silicon [10,11]. Unfortunately, the interference from the silicon in the SiO_2 matrix of BPSG precludes the use of RBS for measuring the phosphorus accurately. We have therefore developed a nuclear reaction analysis (NRA) method based upon the simultaneous measurement of yields from the $^{31}P(\alpha,p_0)^{34}S$ (Q = 0.63 MeV) and $^{10}B(\alpha,p_0)\,^{13}C$ (Q = 4.06 MeV) reactions using 6.0 MeV

incident alpha particles. This method achieves an acceptable combination of speed and accuracy for our application.

Experimental:

The centerpiece accelerator at the IBMRL is an EN Tandem Van de Graaff which underwent Pelletron conversion several years ago. Maximum terminal voltage is <7 MV. The NRA of BPSG films was developed at this facility and is performed in one of our general purpose ion beam analysis (IBA) chambers where we can perform NRA, RBS, elastic recoil detection (ERD), particle-induced x-ray emission (PIXE) and ex-vacuo IBA.

Several factors must be considered in order to optimize an (α,p) system for detecting boron and phosphorus in BPSG. The fairly low Q values for the boron and phosphorus (α,p) require the use of stopping foil in front of the particle detector which is of sufficient thickness to stop scattered alpha particles while allowing the reaction product protons to pass. The foil in this particular application should also be thick enough to reduce the background yield by filtering out the protons from the $^{28}P(\alpha,p_0)^{31}P$ reaction off the glass matrix. The incident alpha particle energy and detector angle must be matched with the stopping foil thickness and the reaction yields to produce the best possible energy separation among the detected reaction product protons while simultaneously maintaining the largest possible count rate for the expected (α,p). The yields of the reactions of interest are not overly large, therefore maximizing the detector solid angle is desirable. Table 1 displays the Q value and the calculated energies of the heavy and light reaction products (at laboratory scattering angle of $\theta_{lab} = 135°$) of the reactions of interest in this application. (The only possible light element interference is from the $^{19}F(\alpha,p_0)^{22}Ne$ reaction which is also included in the table). It is clear

that without a stopping foil yield from the $^{11}B(\alpha,p_0)^{14}C$ reaction would be lost in the background from the RBS signal. The last column of Table 1 shows the energy deposited by the reaction particle in a 500 μm thick surface barrier detector after passing through a 107 μm thick Mylar foil. The calculations are for a 6.0 MeV incident energy and a 135° light product reaction angle. 135° was our detector angle of choice for two reasons. First, as can be seen in Figure (1a), at this angle good energy separation of the reaction protons is achieved. Second, a fairly large detector (we are using a 450 mm^2 detector) can be placed at 135° in our IBM-style scattering geometry. Figure (1b) displays the calculated detected energy (at $\theta_{lab} = 135°$) of the reaction protons from the (α,p) reactions off BPSG as a function of incident alpha energy. A 107 micron Mylar stopping foil was used in these calculations also.

As a result of these calculations and our experimental explorations of yield versus incident alpha energy, we selected a 135° laboratory detector angle and a 107 micron thick Mylar for our analysis setup. Considerations of the thickness of BPSG films we needed to analyze, the yield intensity and the relative constancy of the yield over the energy range of interest determine the incident alpha energy. We generally need to analyze BPSG films which are 1.2 μm thick or less. 6.0 MeV was chosen as our incident alpha energy because the yield for boron (from the $^{10}B(\alpha,p_0)^{13}C$ reaction) was essentially constant over a few hundred keV (at 6.0 MeV incident energy the total alpha energy loss in our films is <200 keV) below this energy. The yield from the phosphorus is not constant, but is enhanced at this energy. 5.3 MeV is another good candidate for these analyses using our setup. The yields for both boron and phosphorus are relatively constant over the required energy range there, but are a factor of 2 or more reduced in intensity. Since this would require longer data

collection time for each sample we chose instead to deal with the non-constant phosphorus versus energy yield around 6.0 MeV in our data analysis.

Figure (2) shows three spectra collected using the experimental setup we have described. The targets were (1) a 306 nm thick BSG film with approximately 5% (by weight) concentration, (2) a 490 nm thick PSG film with approximately 5% phosphorus and a 500 nm thick glass film (essentially SiO_2) deposited by the same TEOS (from a tetraethylorthoysilicate precursor) method as the BPSG films but with no boron or phosphorus doping. In the spectra the $^{10}B(\alpha,p_0)^{13}C$, $^{31}P(\alpha,p_0)^{34}S$ and $^{11}B(\alpha,p_0)^{14}C$ peaks are clearly well separated. It can also been seen, as predicted by the calculations from Figure 1, that the $^{11}B(\alpha,p_0)^{14}C$ and $^{10}B(\alpha,p_1)^{13}C$ peaks overlap such that they are inseparable. The $^{31}P(\alpha,p_1)^{34}S$ and the $^{10}B(\alpha,p_2)^{13}C$ and $^{10}B(\alpha,p_3)^{13}C$ yields also overlap each other and may even contribute some small level of background to the $^{11}B(\alpha,p_0)^{14}C$ and $^{10}B(\alpha,p_1)^{13}C$ peak. The low energy peak (below channel 150) in the spectra is clearly attributable to the $^{28}Si(\alpha,p_0)^{31}P$ reaction since it is the primary element of the TEOS spectrum. Calculations predicted that these protons would not penetrate 107 micrometers of Mylar. This indicates that combination of the stopping power of protons in Mylar and the nominal thickness of our foil are about off by about 10% from the predictions.

The clear separation and extremely low background level of the $^{10}B(\alpha,p_0)^{13}C$, $^{31}P(\alpha,p_0)^{34}S$ peaks had led us to use these reactions for our analyses of the BPSG films. It is noted that the $^{11}B(\alpha,p_0)^{14}C$ + $^{10}B(\alpha,p_1)^{13}C$ total yield in Figure (2) is significantly greater than that for $^{10}B(\alpha,p_0)^{13}C$ (about 6x greater at 6.0 MeV) and should therefore afford better sensitivity and accuracy. It is also true that the overlap of the $^{10}B(\alpha,p_1)^{13}C$ with the $^{11}B(\alpha,p_0)^{14}C$ yield should not affect measurements based upon standards assuming the

$^{11}B/^{10}B$ ratio is constant across samples. Our experience however, has been that results from the $^{11}B(\alpha,p_0)^{14}C + ^{10}B(\alpha,p_1)^{13}C$ total yield are less consistent, probably due to changing background levels. In addition, the $^{11}B(\alpha,p_0)^{14}C + ^{10}B(\alpha,p_1)^{13}C$ total yield is not nearly as constant versus alpha energy (at around 6.0 MeV) as is that from $^{10}B(\alpha,p_{1,2})^{13}C$. It may be that with a few micrometers more foil, or a lower incident alpha energy (~5.3 MeV) where the products of the $^{10}B(\alpha,p_{1,2})^{13}C$, the $^{28}Si(\alpha,p_0)^{31}P$ and the $^{31}P(\alpha,p_1)^{34}S$ reactions are no longer able to pass through the foil to the detector, that the $^{11}B(\alpha,p_0)^{14}C + ^{10}B(\alpha,p_1)^{13}C$ reactions would prove better for boron analysis. If the background is due to multiple scattering from the $^{31}P(\alpha,p_0)^{34}S$ reaction however the $^{10}B(\alpha,p_0)^{13}C$ reaction would likely remain the better choice.

Analysis:

Prior to our development of this NRA technique, the fab at Sandia National Laboratories calibrated its B/P ratios in BPSG films via ICPS performed by an outside company. ICP results on some "standard" films have been used to calibrate our NRA. We plan to have periodic recalibration performed by the same method. Extremely accurate film thickness data obtained in the fab process with ellipsometry measurements are provided to us for each sample. The boron and phosphorus content in the films is assumed to be constant with depth. Prior to each analysis run on new samples the standard samples are analyzed to ensure that the measurements are consistent. In this way any problems with current integration, targeting, or the experimental setup can be eliminated. Figure (3) displays plots of the yield versus film thickness for a set of "standard" BPSG films. The constant cross-section of the $^{10}B(\alpha,p_0)^{13}C$ reaction is clearly evident from the linear nature of the boron

yield data. Since the cross-section is constant the areal density of boron in the sample film (N_B) is simply:

$$N_B = [(N_{BSTD})(Y)(t_{STD})]/[(Y_{STD})(t)] \qquad [1]$$

where N_{BSTD} is the areal density of the boron in the standard, Y and Y_{STD} are the boron yields and t and t_{STD} are the measured film thickness of the sample and the standard respectively. It is a trivial matter to convert boron yield and thickness data to the units of weight % desired by our fab. We assume the same film density of 2.1 g/cm^3 for all the films and that all films contain the natural B abundance (^{11}B at 80.1% and ^{10}B at 19.9%).

It is also evident in Figure (3) that the $^{31}P(\alpha,p_0)^{43}S$ cross-section decreases with energy below 6.0 MeV. The phosphorus is also not a constant function of phosphorus dopant level from one thickness to another. This indicates that the reaction cross-section is sensitive to the relatively small differences in stopping power in the differently doped films, especially at thicknesses greater than a micrometer. In this case we have performed a three dimensional fit of yield, film thickness and weight % phosphorus to the data in Figure (3). The fit is of the form:

$$\%P=(a+b\ln x+c\ln y+d(\ln y)2)/(1+e\ln x+f(\ln x)2+g\ln y+h(\ln y)2) \qquad [2]$$

where x is thickness, y is the yield data and a through h are fitting parameters. While no particular physical insight can be gained from the form of the fit, it is very useful for predicting the weight % phosphorus in a particular film given the ellipsometry thickness measurement and the $^{31}P(\alpha,p_0)^{43}S$ NRA yield data. The 95% prediction levels for the fit are within 2% of our data in the thickness range from 0.1 to 1.3 μm.

<u>Summary:</u>

We have achieved our goal of developing a quick, single energy, NRA technique for measuring the boron and phosphorus in BPSG films 0.2 to 1.3 μm thick. Film thickness is measured by ellipsometry as part of the fabrication process of the films. Typical NRA measurements are for 20 μC of integrated charge per (about 6 minutes per sample at our typical 50 nA beam current) sample using 6.0 MeV $^{4}He^{+}$, a 450 mm^2, 500 μm thick surface barrier detector at 135°, and a ~107 μm Mylar ranging foil. Analyses of BPSG films containing 5% each of boron and phosphorus, produce yields in the 15000 count range for the combined $^{11}B(\alpha,p_0)^{14}C$ and $^{10}B(\alpha,p_1)^{13}C$ reactions, around 12000 counts for the $^{31}P(\alpha,p_0)^{34}S$ reaction and about 2000 counts for the $^{10}B(\alpha,p_0)^{13}C$ reaction. Background counts in the latter two reactions, as measured off TEOS silicate-glass films containing no boron or phosphorus doping, are independent of dopant level and consistently measure less than 25 counts per sample under the same collection conditions. The background of the combined $^{11}B(\alpha,p_0)^{14}C$ and $^{10}B(\alpha,p_1)^{13}C$ reactions does not appear to be independent of dopant levels with this experimental setup. Quantification of the boron and phosphorus in the films is performed by normalization with measurements of "standard" BPSG film samples. The analysis of phosphorus involved a three-dimensional fit of yield, thickness and weight % phosphorus data from a "standard" matrix of BPSG films. Accuracy of the method ranges from better than 5% for the more heavily doped films to 8 to 10% for the lightly doped glass. The lower dopant limits for quantitative measurements at the 10% accuracy level are 0.1% (weight) for boron and about one third that for phosphorus.

Reaction	Q Value [MeV]	Heavy Product Excited Energy Level [MeV]	Light Product Emitted Energy [MeV]	Light Product Detected Energy [MeV]
$^{31}P(\alpha,p_0)^{34}S$	0.627	0.000	5.292	4.033
$^{31}P(\alpha,p_1)^{34}S$	-1.500	2.128	3.321	1.117
$^{31}P(\alpha,p_2)^{34}S$	-2.677	3.304	2.243	nd
$^{11}B(\alpha,p_0)^{14}C$	0.784	0.000	3.822	2.033
$^{10}B(\alpha,p_0)^{13}C$	4.062	0.000	6.372	5.312
$^{10}B(\alpha,p_1)^{13}C$	0.973	3.089	3.792	1.984
$^{10}B(\alpha,p_2)^{13}C$	0.378	3.685	3.303	1.078
$^{10}B(\alpha,p_3)^{13}C$	0.208	3.854	3.165	0.753
$^{16}O(\alpha,p_0)^{19}F$	-8.114	-	-	nd
$^{28}Si(\alpha,p_0)^{31}P$	-1.916	0.000	2.838	nd
$^{28}Si(\alpha,\alpha)^{28}Si$	0.000	0.000	3.668	nd
$^{31}P(\alpha,\alpha)^{31}P$	0.000	0.000	3.849	nd
$^{19}F(\alpha,p_0)^{22}Ne$	1.674	0.000	5.579	4.382

Table 1. Nuclear reactions of interest in analyzing BPSG. Also shown are the reaction Q-values, energy levels of the heavy reaction product and the light reaction product [12,13]. Laboratory scattering angle is 135°. The *light product detected energy* is the energy the light reaction product deposits in a 500 micron thick silicon surface barrier detector after passing through a 107 micrometers thick Mylar foil. (calculated following Ziegler [14]) *nd* indicates that calculations show the particle does not fully penetrate the Mylar foil.

FIGURE CAPTIONS

Figure (1). Plots of the calculated energy deposited in a 500 μm depletion depth silicon surface barrier detector versus the incident alpha particle energy (Figure 1B) and the detector reaction angle at incident alpha energy of 6.0 MeV (Figure 1a) for the (α,p) reactions off BPSG. Calculations include effects of a 107 μm Mylar ranging foil. Maximum possible energy separation of reaction products is achieved at moderate back angles ($100° < \theta < 150°$). Separation of the $^{11}B(\alpha,p_0)^{14}C$ and $^{10}B(\alpha,p_1)^{13}C$ products is never achieved. Background from the $^{28}Si(\alpha,p_0)^{34}S$ reaction is eliminated by the foil for alpha energies below 5.3 MeV. Note that at small forward angles the entire energy of the $^{10}B(\alpha,p_0)^{13}C$ proton is not deposited within the detector depletion layer.

Figure (2). Multi-channel analyzer spectra of (α,p) NRA on doped silicate-glass films. Incident alpha energy was 6.0 MeV, detector angle is 135°. A 450 mm^2 surface area, 500 μm thick surface barrier detector with an ~107 μm Mylar ranging foil was used. Spectra were collected for 10 μC. Spectra are from a boron doped glass (BSG), a phosphorus doped glass (PSG) and an undoped glass (TEOS). All films are around 0.5 μm thick. Dopant levels are around 4% by weight.

Figure (3). Plots of $^{31}P(\alpha,p_0)^{34}S$ and $^{10}B(\alpha,p_0)^{13}C$ yield versus film thickness for silicate-glass films doped with either phosphorus (at 2%, 4% or 5% by weight), or boron at (1% or 5%). The linearity of the B yield data indicates that the cross-section for this reaction is constant over the thickness of these films. The cross-section of the P reaction is clearly not constant. A three dimensional fit to the P yield data is used to determine weight %P in the films.

LITERATURE CITED

[1] S.M. Sze, Semiconductor Devices Physics and Technology, John Wiley & Sons, New York, 1985.

[2] K. Nassau, R.A. Levy and D.L. Chadwick, J. of the Electrochemical Society, v. 132(#2) (1985)409.

[3] K.J. Uram, J.K. Shugrue and N.P. Sandler, in: V.J. Kapoor and W.D. Brown (Eds.), Proceedings Of The Third Symposium On Silicon Nitride And Silicon Dioxide Thin Insulating Films, Dielectric Science and Technology and Electronics Divisions Proceedings Volume 94-16, The Electrochemical Society, 1994.

[4] G.D. Mea, Nucl. Instr. And Meth. B 15 (1986) 495.

[5] L.C. McIntyre Jr., J.A. Leavitt, B. Dezfouly-Arjomandy and J. Oder, Nucl. Instr. And Meth. B 35 (1988) 446.

[6] E. Ligeon, M. Bruel, A. Bontemps, G. Chambert and J. Monnier, J. Radioanal. Chem., 16 (1973) 537.

[7] N. Moncoffre, Nucl. Instr. And Meth. B 66 (1992) 126.

[8] A.E. Pillay and M. Peisach, Nucl. Instr. And Meth. B 66 (1992) 226.

[9] L.C. McIntyre Jr., J.A. Leavitt, M.D. Ashbaugh, A. Lin, and J.O. Stoner Jr., Nucl. Instr. And Meth. B 66 (1992) 221.

[10] D.S. Walsh, B.L. Doyle, W.R. Wampler and A.K. Hays, J. Vac. Sci. Technol. A9 (1991) 727.

[11] B.L. Doyle, D.S. Walsh and W.R. Wampler, J. Nucl. Mater. 196-198 (1992) 658.

[12] S.Y. Chu, H. Nordberg, H.B. Firestone and L.B. Ekström, Isotope Explorer 2.23 Computer Code, Lawrence Berkeley National Laboratory, 1999.

[13] A.H. Wapstra and K. Bos, Atomic Data and Nuclear Data Tables, Vol. 19(3), (March, 1977) 185.

[14] J. F. Ziegler, The Stopping and Range of Ions in Matter, vol. 6, Pergamon Press, 1985.

Figure 1A

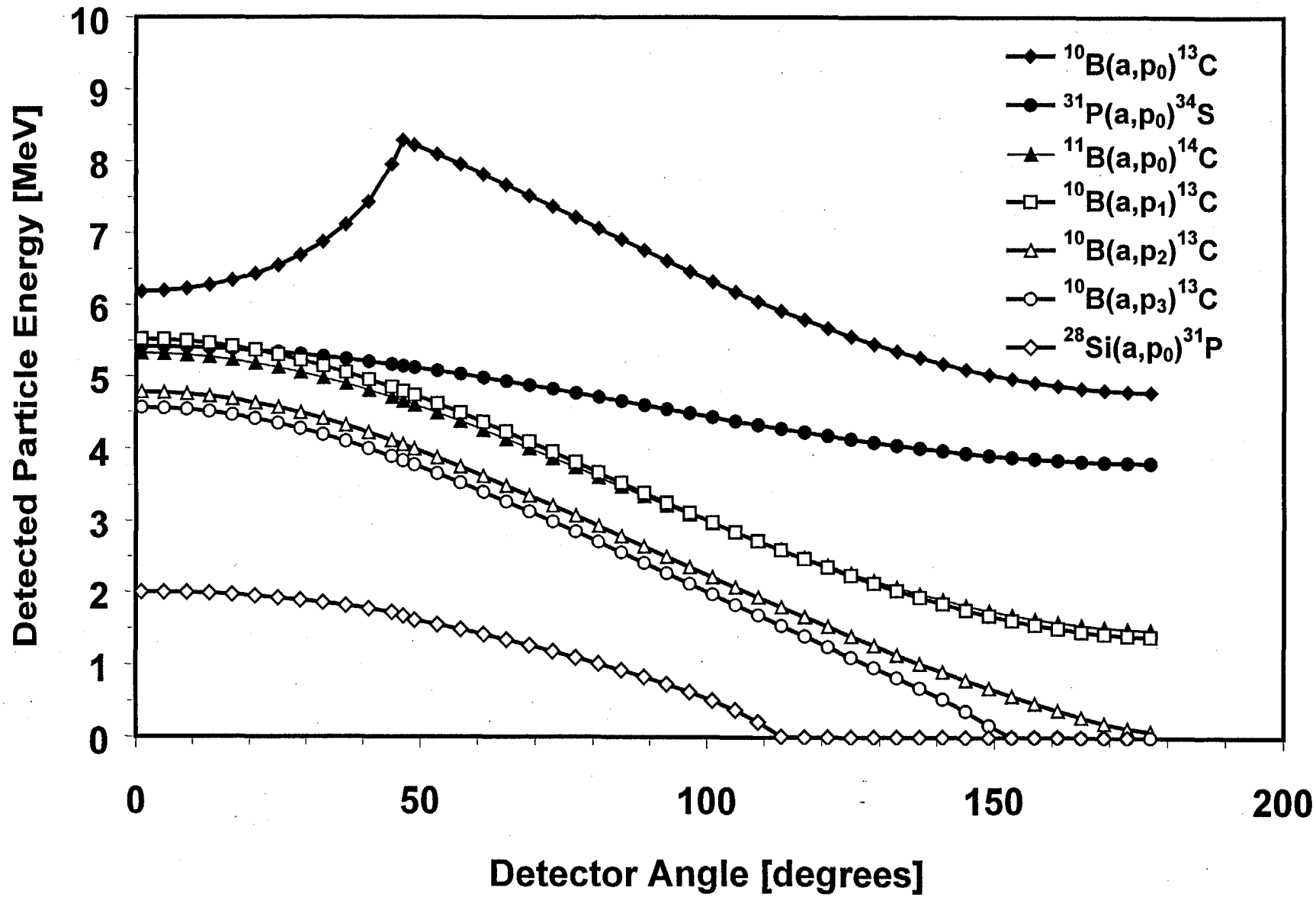
Detected Particle Energy [MeV]
10
9
8
7
6
5
4
3
2
1
0
0
50
100
150
200
Detector Angle [degrees]
$^{10}B(a,p_0)^{13}C$
$^{31}P(a,p_0)^{34}S$
$^{11}B(a,p_0)^{14}C$
$^{10}B(a,p_1)^{13}C$
$^{10}B(a,p_2)^{13}C$
$^{10}B(a,p_3)^{13}C$
$^{28}Si(a,p_0)^{31}P$

Figure 1B

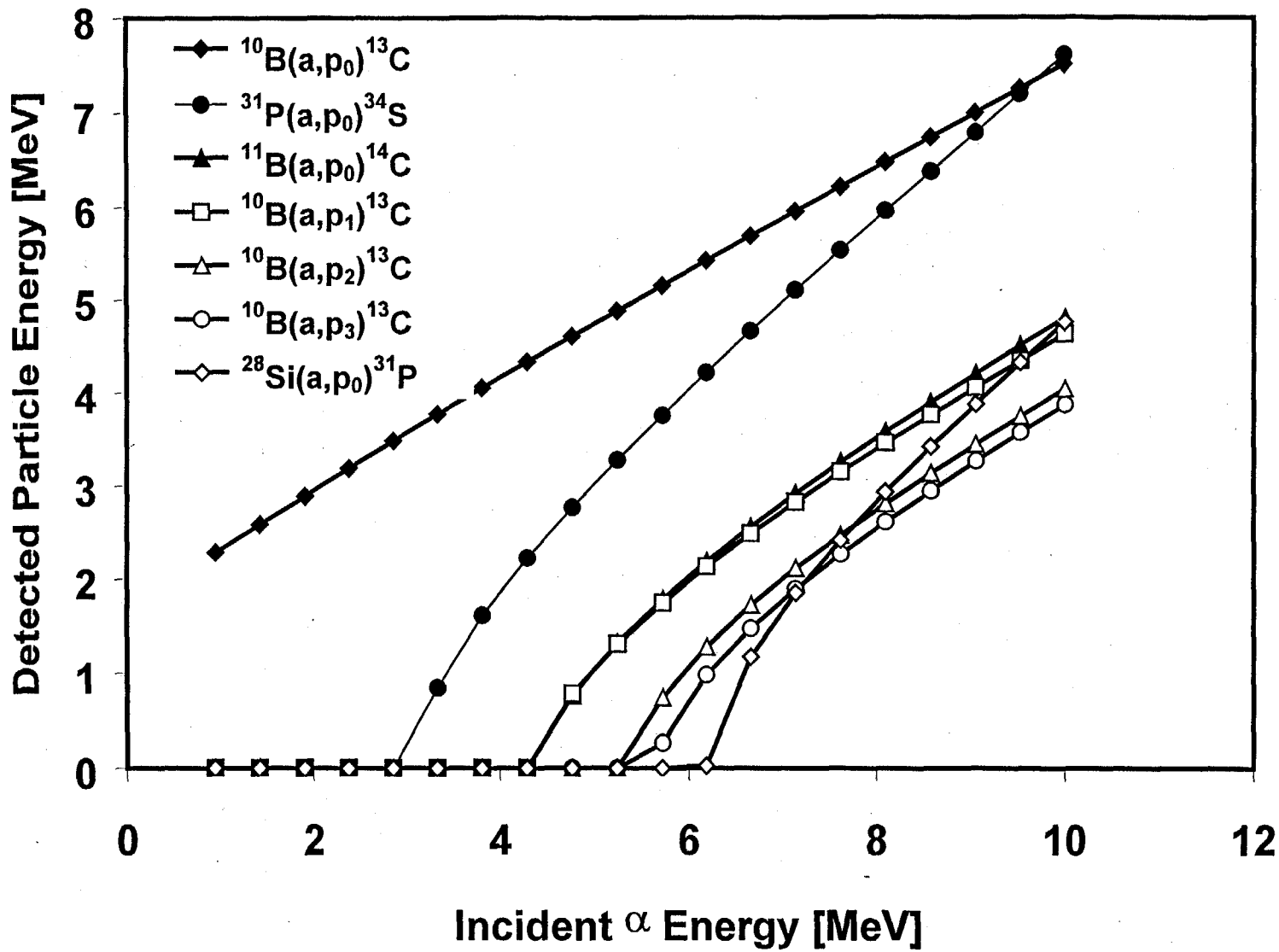
$^{10}B(a,p_0)^{13}C$
$^{31}P(a,p_0)^{34}S$
$^{11}B(a,p_0)^{14}C$
$^{10}B(a,p_1)^{13}C$
$^{10}B(a,p_2)^{13}C$
$^{10}B(a,p_3)^{13}C$
$^{28}Si(a,p_0)^{31}P$
Detected Particle Energy [MeV]
Incident α Energy [MeV]
0
1
2
3
4
5
6
7
8
0
2
4
6
8
10
12

Figure 2

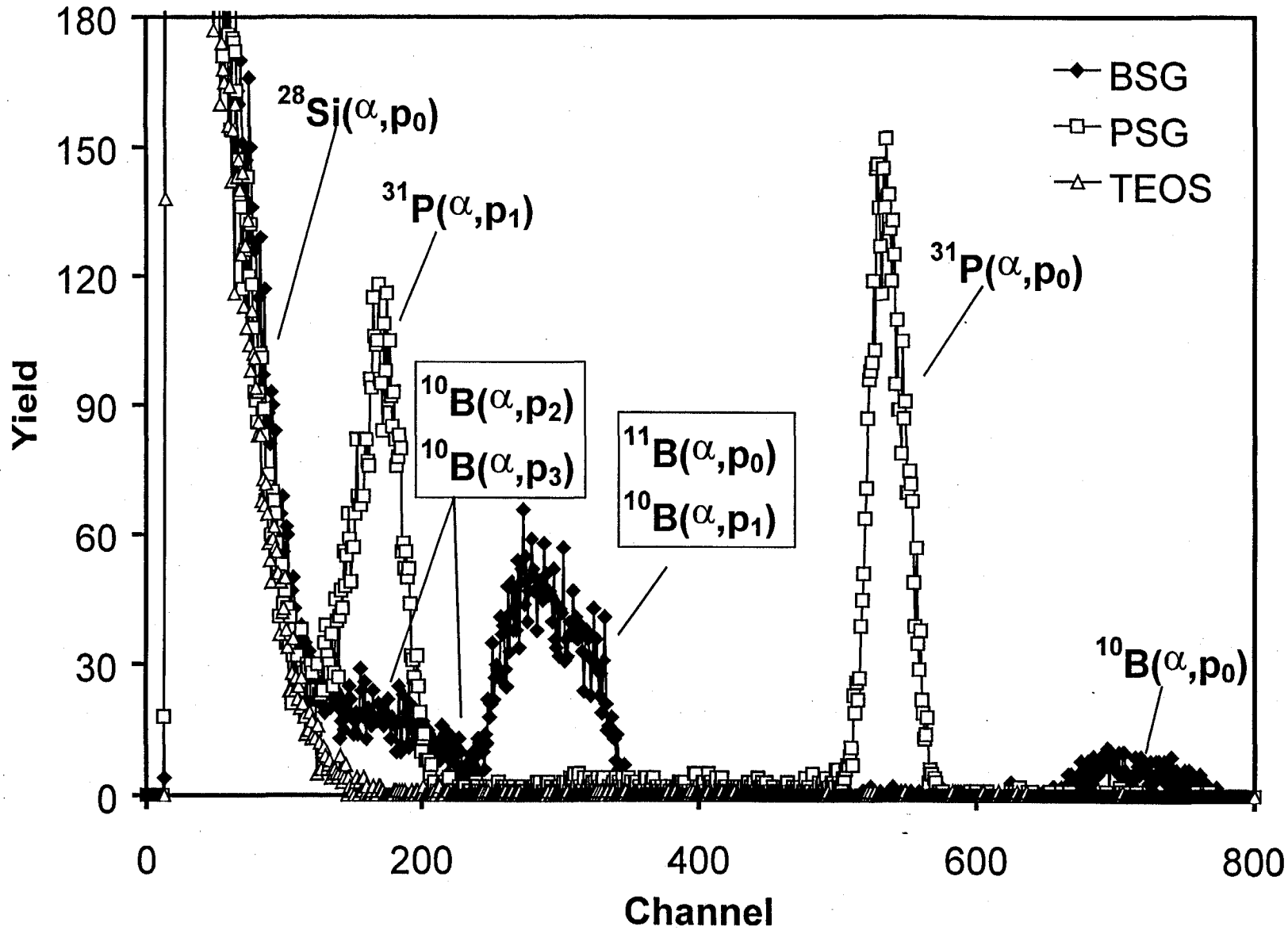
180
150
120
90
60
30
0
Yield
0
200
400
600
800
Channel
BSG
PSG
TEOS
$^{28}Si(\alpha,p_0)$
$^{31}P(\alpha,p_1)$
$^{10}B(\alpha,p_2)$
$^{10}B(\alpha,p_3)$
$^{11}B(\alpha,p_0)$
$^{10}B(\alpha,p_1)$
$^{31}P(\alpha,p_0)$
$^{10}B(\alpha,p_0)$

Figure 3

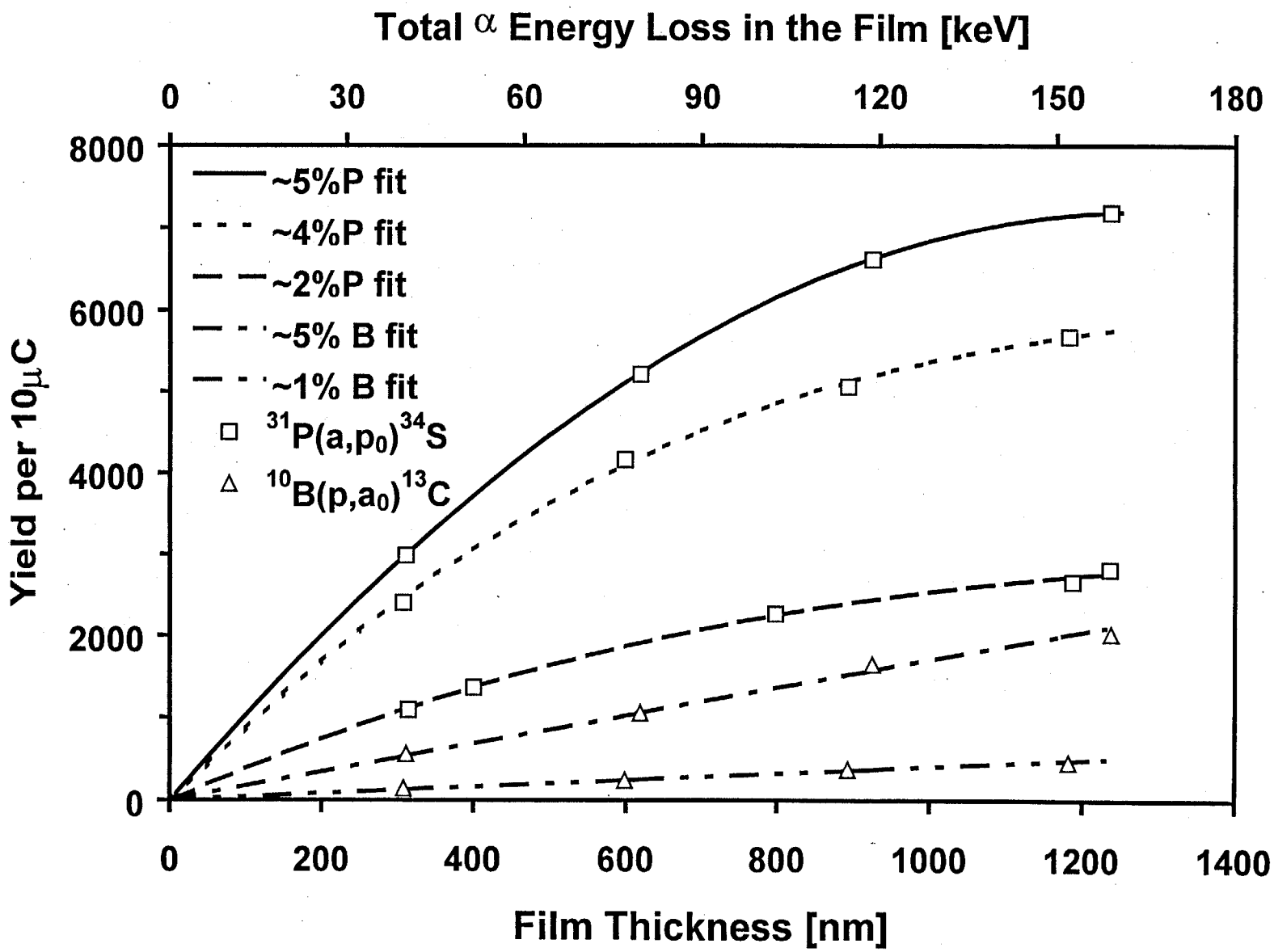
Total α Energy Loss in the Film [keV]
0
30
60
90
120
150
180
8000
6000
4000
2000
0
Yield per 10μC
~5%P fit
~4%P fit
~2%P fit
~5% B fit
~1% B fit
31P(a,p0)34S
10B(p,a0)13C
0
200
400
600
800
1000
1200
1400
Film Thickness [nm]